Aerodynamic property and filtration evaluation of airborne graphene nanoplatelets with plate-like shape and folded structure

Author(s):
Gao, Hanchao; He, Weidong; Yu, Ranxue; Hammer, Tobias; Xu, Guangbiao; Wang, Jing

Publication date:
2020-11-15

Permanent link:
https://doi.org/https://doi.org/10.3929/ethz-b-000424105

Originally published in:
Separation and Purification Technology 251, https://doi.org/10.1016/j.seppur.2020.117293

Separation and Purification Technology 251 (2020) 117293

Contents lists available at ScienceDirect

Separation and Purification Technology

journal homepage: www.elsevier.com/locate/seppur

Monograph

Aerodynamic property and filtration evaluation of airborne graphene nanoplatelets with plate-like shape and folded structure

Hanchao Gao[a,b,c], Weidong He[b,c], Ranxue Yu[a,b,c], Tobias Hammer[b,c], Guangbiao Xu[a,*], Jing Wang[b,c,*]

[a] Key Laboratory of Textile Science & Technology, Ministry of Education, College of Textiles, Donghua University, No. 2999 North Renmin Road, Songjiang, Shanghai 201620, China
[b] Institute of Environmental Engineering, ETH Zurich, 8093 Zurich, Switzerland
[c] Advanced Analytical Technologies, Empa, Ueberlandstrasse 129, 8600 Dübendorf, Switzerland

ARTICLE INFO

Keywords:
Graphene nanoplatelets
Folded structure
Aerodynamic property
Filtration efficiency
Quality factor

ABSTRACT

With the wide applications of graphene nanoplatelets (GNPs) in the industries, more concerns are raised about the effectiveness of filtration technology to control GNPs release during manufacturing and handling processes. Accurate prediction of the capture efficiency of airborne GNPs is significant to avoid occupational exposure. Herein, the aerodynamic property and filtration mechanisms of airborne GNPs with plate-like shape and folded structure were studied. Different equivalent diameters of GNPs (aerodynamic diameter d_a, mobility diameter d_m) were derived and used to describe diverse mechanisms in the filtration model. The capture efficiency of plate-like GNPs and sphere-like NaCl particles was measured with Nuclepore membranes and nanofibrous membranes to assess the particle shape effect during filtration. The plate-like GNPs showed higher capture efficiency due to the larger interception length. SEM measurement showed that not only planar GNPs, GNPs with folded structure also occurred due to the large lateral size to thickness ratio and strong mechanical stimulation in the atomization process. For GNPs with aerodynamic diameter of 0.5 – 0.9 μm, the capture efficiency for folded GNPs decreased by 20 – 30% according to the analytical calculation. In addition, the effects of membrane structural parameters (Nuclepore membrane pore radius, fiber diameter, solidity) on the quality factor (Q_f) were systematically analyzed to evaluate the overall filtration performance. This study not only elucidates the effect of plate-like shape and folded structure on the aerodynamics of airborne GNPs, but also contributes to better design of Nuclepore and nanofibrous membranes to improve the filtration performance of plate-like particles.

1. Introduction

Graphene nanoplatelets (GNPs) are promising nanomaterials and widely used in commercial products attributed to the rapid development of nanotechnology in the past decades. With wide applications in electronics [1], sensors [2], composite materials [3] and biotechnology [4], a growing concern about possible GNPs release and potential adverse human health effect has been raised. GNPs can be released into the environment in various phases of products life time, including production, service life and disposal [5,6]. Available data indicate that nanoparticles could be released during abrasion [7,8], drilling [9], exposure to UV light [10] and combustion of nanoparticle composite materials [11]. There are some studies about GNPs transportation in aquatic or soil environment [12,13], however, researches about the transport and deposition of airborne GNPs are far from adequate. Released GNPs can be inhaled and deposit in the respiratory tract of human, and the failed engulfment of large GNPs by the macrophage cells would result in frustrated phagocytosis and inflammation [14]. Filtration is one of the primary technologies that can effectively remove nanoparticles from air and minimize the detriment to human health [15–20]. Precise prediction of airborne GNPs capture efficiency is very significant to avoid occupational exposure during manufacturing and handling processes.

The filtration performance of filters is usually characterized by challenging with sphere-like particles such as sodium chloride (NaCl) and dioctylpthalate (DOP). However, the particle shape is a significant parameter which strongly affects the particle transportation and deposition in filters [21]. Compared to spherical particles, GNPs exhibit

* Corresponding authors at: Key Laboratory of Textile Science & Technology, Ministry of Education, College of Textiles, Donghua University, Shanghai 201620, China (G. Xu). Institute of Environmental Engineering, ETH Zurich, 8093 Zurich, Switzerland (J. Wang).
E-mail addresses: guangbiao_xu@dhu.edu.cn (G. Xu), jing.wang@ifu.baug.ethz.ch (J. Wang).

https://doi.org/10.1016/j.seppur.2020.117293
Received 12 March 2020; Received in revised form 19 June 2020; Accepted 22 June 2020
Available online 27 June 2020

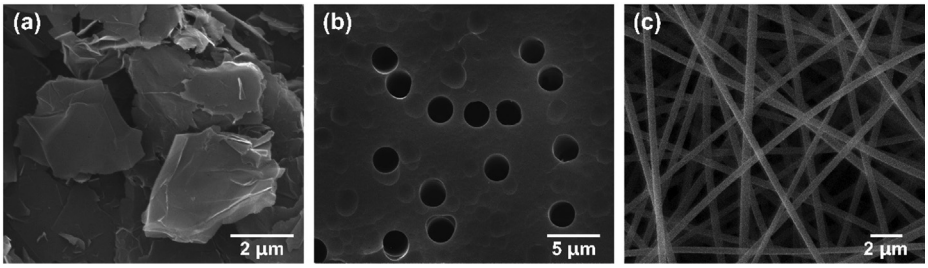

Fig. 1. SEM images of (a) graphene nanoplatelets, (b) Nuclepore membrane with pore diameter of 3 μm, (c) PAN electrospun membrane.

unique aerodynamic properties due to the plate-like shape. However, researches about how the plate-like shape affects GNPs filtration are far from adequate. There are some studies about filtration of high aspect ratio fiber-like particles, such as asbestos and carbon nanotubes (CNTs). Feigley [22] modified the classic filtration theory to develop a model for the deposition of asbestos in fibrous membranes. Chen et al. [23] investigated the CNTs filtration mechanisms using the modified capillary tube model and found that the penetration of CNTs was closely related to the particle effective length, mobility diameter and density. Previous researches [24–26] indicated that the major difference between fiber-like particles and spheres was caused by the interception mechanism, for which the geometric diameter played a key role for elongated particles. However, up to now, studies on the filtration of airborne two-dimensional GNPs are scarce, the details about the deposition mechanisms and the plate-like shape effect have not been investigated.

GNPs tend to fold due to the large lateral size to thickness ratio and out-of-plane flexibility [27,28]. Several studies investigated the folding and aggregation of graphene nanomaterials in aquatic and soil environment [12,13,29]. The effects of solution chemistry (such as pH, ionic strength, salt type) and soil properties (such as surface area, charge status) on the stability of graphene nanomaterials were presented. Folding transforms GNPs into more intricate shapes and influences particle aerodynamic property. However, studies about how the folded structure influences airborne GNPs transportation and deposition are scarce. It is significant to take folding into consideration for better aerodynamics analysis and more accurate prediction of the capture efficiency of plate-like GNPs.

The filtration performance not only depends on particle properties, but also the filter structure. There are two most important types of filters: porous membrane filters and fibrous filters. One type of commonly used porous membrane is Nuclepore membrane which has microscopic holes with uniform diameter perpendicular to the filter surface. Nuclepore filters with well-defined and homogenous microstructure, which can be accurately described by the capillary tube model, facilitate the study of particle deposition mechanisms. Fibrous filters are mats composed of randomly orientated fibers. In recent years nanofibrous membranes have become one of the most promising candidates in the filtration industry. On one hand, the filtration efficiency is significantly enhanced as the fiber diameter decreases to the nanometer-scale [30]. On the other hand, the slip flow effect diminishes the friction between air molecules and nanofibers and led to the decreased resistance [31,32]. However, most of the researches are focused on the capture of spherical particles or fiber-like particles, studies about how the plate-like shape influences particle transportation through porous and fibrous membranes are still scarce.

In the present work, the aerodynamic property and filtration mechanisms of airborne GNPs with plate-like shape and folded structure were studied. The capture efficiencies of GNPs and NaCl particles by Nuclepore membranes and nanofibrous membranes were compared to evaluate the particle shape effect. Different equivalent diameters (aerodynamic diameter d_a, mobility diameter d_m, geometrical diameter d_g) of GNPs were derived and used to account for diverse mechanisms in the filtration model. Besides planar GNPs, GNPs with folded structure also existed due to the powerful mechanical stimulation during the atomization process. Analytical models based on the capillary tube theory and single-fiber theory were used to predict the penetration difference among planar GNPs, folded GNPs and spheres with the particle aerodynamic diameter from 0.07 to 10 μm. In addition, the effects of Nuclepore membrane pore radius, nanofiber diameter and solidity on the quality factor (Q_f) were systematically investigated for better membrane design with optimized filtration performance for plate-like particles.

2. Materials and experiments

2.1. Materials

The graphene nanoplatelets (GNPs) were purchased from XG Science Inc., USA. They were grade M GNPs consisting of short stacks of graphene sheets with plate-like shape. The average lateral size was about 5 μm (Fig. 1a). The true density was 2.2 g cm^{-3} and surface area was 120 to 150 m^2 g^{-1}. The Nuclepore filters with pore diameter of 3 μm (WHA-111112, Whatman International Ltd., UK) were used to collect the GNPs for SEM characterization. Nuclepore filters were membrane filters with microscopic holes of uniform diameter, approximately perpendicular to the membrane surface (Fig. 1b). The particles could be captured on the filter surface, on the pore opening or on the walls of the pore. The porosity and thickness of the Nuclepore membrane were 0.14 and 9.9 μm, respectively. Polyacrylonitrile (PAN, M_w = 150000), sodium chloride (NaCl) and N,N-dimethy(formamide) (DMF) were purchased from Sigma Aldrich.

2.2. Fabrication of electrospun membranes

The electrospinning setup was similar to Kuo et al. [33]. 9 wt% PAN solution was prepared by dissolving PAN in DMF and continuously stirred for 8 h. The solution was loaded into a 10 mL syringe with a metal needle possessing inner diameter of 0.41 mm. The solution was fed at a controllable flow rate of 0.8 mL h^{-1} by a syringe pump (NE-300, New Era Pump Systems Inc., USA). A 20 kV voltage was applied to the needle and nanofibers were collected on the aluminum foil with tip-to-collector distance of 20 cm. All electrospinning experiments were conducted at 20 ± 2 °C and 45 ± 5% relative humidity. The morphology of PAN electrospun membranes was characterized by Scanning Electron Microscopy (SEM, Nova NanoSEM 230, Thermo Fisher Scientific, USA) and shown in Fig. 1c. The nanofibers were randomly oriented with the average diameter of 447 ± 54 nm.

2.3. Gnps filtration tests with Nuclepore and nanofibrous membranes

Fig. 2 shows the experimental setup for filtration tests. Firstly, GNPs were dispersed in water with concentration of 0.02 wt% and ultrasonicated for 30 min to avoid agglomeration. Airborne GNPs were generated by atomizing the GNPs suspension using a Collison type atomizer. Then the atomized aerosols went through a diffusion dryer to

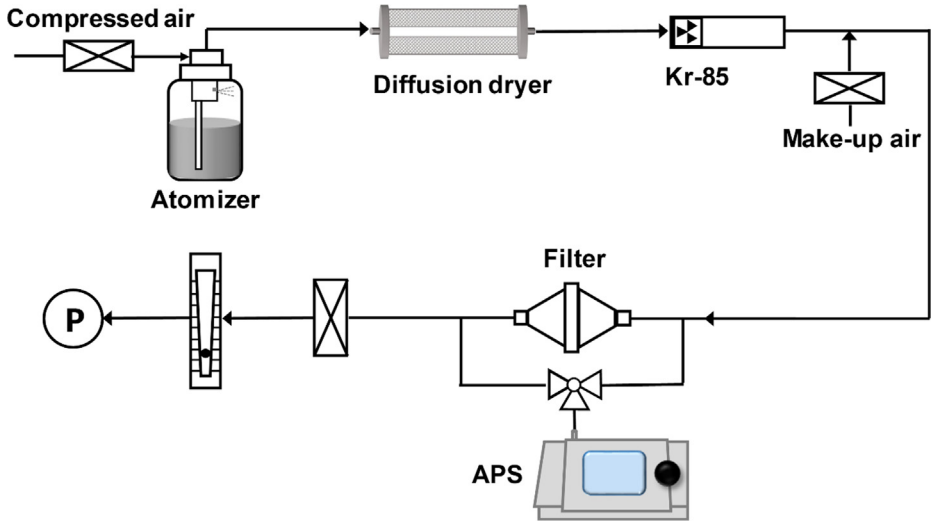

Fig. 2. Experimental setup for airborne particles filtration tests.

remove the water vapor. A neutralizer (Kr-85) was used to minimize the electrostatic effect on filtration. The aerodynamic size distribution and concentration of GNP aerosol were measured by an Aerodynamic Particle Sizer (APS). By adjusting the three-way valve located in front of the APS inlet, the upstream particle concentration C_{up} and downstream particle concentration C_{down} were measured, and the filtration efficiency was calculated as $E = 1 - C_{down}/C_{up}$. The face velocity during filtration was 5 cm s^{-1}. In addition, in order to compare the capture efficiency between GNPs and sphere-like particles, airborne NaCl particles were also generated by atomizing 0.1 wt% NaCl solution. The experimental data and model results of the capture efficiency between GNPs and NaCl particles were compared.

3. Theoretical models

3.1. Equivalent diameters derivation using analytical expressions

For non-spherical particles, the drag force and settling velocity not only depended on particle size but also particle shape [34]. Different equivalent diameters were needed to account for different mechanisms (interception, impaction, diffusion) during filtration. Additionally, the equivalent diameters of folded GNPs were also derived by assuming that a totally folded GNP was a particle with half surface area and doubled thickness of planar GNP.

Aerodynamic diameter d_a is a key parameter for characterizing particle deposition by inertial impaction. The oblate spheroid has been widely used in the aerodynamics calculation for plate-like particles in previous research [35–38]. Cheng et al. [36] studied the aerodynamic properties of plate-like talc particle and established the relationship between aerodynamic diameter and projected area diameter. Tomb et al. [37] derived the correlation between Stokes diameter and volume diameter of plate-like mica particles. The above studies showed that the shape factor of plate-like particle was in good agreement with experimentally determined shape factor for oblate spheroid, indicating oblate spheroid was a good approximation for the aerodynamic analysis of plate-like particles. In addition, particle random orientation should be considered during calculation. In our study the drag force of GNPs was calculated based on the drag force model [39] determined for an oblate spheroid ($\frac{x^2}{a^2} + \frac{y^2}{a^2} + \frac{z^2}{b^2} = 1$). In addition, the aerodynamic drag force was also influenced by the orientation of particles. Under the assumption that the thickness of the particle was infinitely thin, the drag force F_{D1} of a GNP perpendicular to the direction of motion was calculated as:

$$F_{D1} = 8\mu V d_g \tag{1}$$

The drag force F_{D2} of a GNP parallel to the direction of motion was calculated as:

$$F_{D2} = \frac{16}{3}\mu V d_g \tag{2}$$

with d_g: GNPs geometrical diameter, V: velocity of GNPs, μ: gas viscosity.

For a spherical particle with unit density, the drag force F_{DS} was calculated as $F_{DS} = 3\pi\mu V d_a$. The aerodynamic diameter is the diameter of a unit density sphere that has the same settling velocity as the particle under consideration. Therefore, by equaling the settling velocity of a sphere with that of a GNP, the aerodynamic diameter d_{a1} of GNP with perpendicular orientation and the aerodynamic diameter d_{a2} of GNP with parallel orientation were calculated as:

$$d_{a1} = \sqrt{\frac{9\pi\rho_p d_g t_p}{16\rho_0}} \tag{3}$$

$$d_{a2} = \sqrt{\frac{27\pi\rho_p d_g t_p}{32\rho_0}} \tag{4}$$

with t_p: thickness of GNPs, ρ_p: density of GNPs (2.2 g cm^{-3}), ρ_0: unit density (1 g cm^{-3}).

For a GNP with random orientation, the aerodynamic diameter d_a was calculated as:

$$d_a = d_{a1} sin^2\varphi + d_{a2} cos^2\varphi \tag{5}$$

with $sin^2\varphi = 2/3$ *and* $cos^2\varphi = 1/3$, which were derived by Fuchs [40] by neutralizing the resistance in all directions of the polar axis.

The mobility diameter d_m is important for evaluating particle motion due to diffusion. The mobility diameter is the equivalent diameter of a spherical particle that has the same terminal electrostatic velocity in the electric field as the particle under consideration. When a charged particle with n elementary units of charge is placed in an electric field with field intensity E, it is acted upon by the electrostatic force F_E calculated as$F_E = neE$.The particle reached terminal electrostatic velocity as the electrostatic force balanced the drag force. By equaling the terminal electrostatic velocity of sphere with that of GNP, the mobility diameter d_{m1} of GNP with perpendicular orientation and the mobility diameter d_{m2} of GNP with parallel orientation were calculated as:

$$d_{m1} = \frac{8d_g}{3\pi} \tag{6}$$

$$d_{m2} = \frac{16d_g}{9\pi} \tag{7}$$

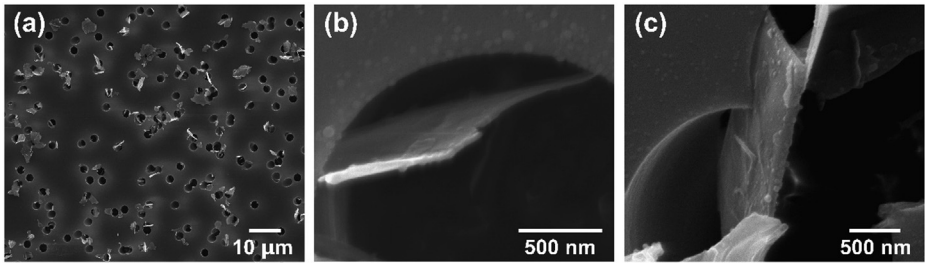

Fig. 3. SEM images of (a) airborne GNPs collected on the Nuclepore filter, (b) a planar GNP and (c) a folded GNP captured at the pore entrance of Nuclepore membrane.

For a GNP with random orientation, the mobility diameter d_m was calculated as:

$$d_m = d_{m1}sin^2\varphi + d_{m2}cos^2\varphi \tag{8}$$

3.2. Capillary tube filtration model for Nuclepore membranes

For Nuclepore filters with microscopic circular holes with uniform diameter, the capillary tube model was used to predict particle collection characteristics [41]. Collection efficiencies due to four filtration mechanisms were considered: impaction on the filter surface ε_i, interception on the pore opening ε_R, diffusion on the walls of the pore ε_D, and diffusion on the front surface of the filter ε_{DS}. Different equivalent diameters relevant to each deposition mechanism was used in the capillary tube model to account for particle shape effect. The aerodynamic diameter d_a, geometric diameter d_g and mobility diameter d_m were used to calculate the filtration efficiencies attributed to impaction, interception and diffusion, respectively. The detailed analytical expressions for efficiencies calculation were shown in the Supplementary Information. The total filtration efficiency ε_T attributed to the above mechanisms was calculated as:

$$\varepsilon_T = 1 - (1 - \varepsilon_i)(1 - \varepsilon_R)(1 - \varepsilon_D)(1 - \varepsilon_{DS}) \tag{9}$$

The pressure drop across the Nuclepore membrane was calculated by the Hagen-Poiseuille equation [41]:

$$\Delta p = p_1 - p_1\sqrt{1 - 5.093\frac{\mu t U_0}{p_1 r_0^4 N_p}} \tag{10}$$

with p_1: gas pressure upstream of the membrane, μ: air dynamic viscosity, t: membrane thickness, U_0: face velocity, r_0: pore radius, N_p: number of pores per unit surface area.

3.3. Single-fiber filtration theory for fibrous membranes

The single-fiber filtration model with slip effect was used for analytical calculation of the filtration efficiency of fibrous membranes. Three different mechanisms (interception, impaction and diffusion) were considered in the filtration model, and the detailed calculation equations were shown in the Supplementary Information. The total single-fiber efficiency E_T was the summation of efficiency due to interception, impaction and diffusion:

$$E_T = E_R + E_I + E_D \tag{11}$$

The penetration of the membrane was calculated as:

$$P = \exp\left(-\frac{4\alpha E_T t}{\pi d_f(1-\alpha)}\right) \tag{12}$$

with α: membrane solidity, d_f: fiber diameter, t: membrane thickness.

In order to accurately predict the pressure drop of nanofibrous membranes, the fiber random distribution and slip effect should be considered [42]. One widely used equation for pressure drop of fibrous membranes at continuum regime Δp_c obtained from empirical data and including the effects of fiber random orientation and neighboring interference, was given by Davies [43]:

$$\Delta p_c = \mu U_0 t[64\alpha^{1.5}(1 + 56\alpha^3)]/{d_f}^2 \text{for}(0.006 < \alpha < 0.3) \tag{13}$$

with μ: air dynamic viscosity, U_0: face velocity, t: membrane thickness, d_f: fiber diameter.

For nanofibrous membrane, as the nanofiber diameter d_f was comparable with the mean free path of air molecules λ, the slip effect on the fiber surface became significant and a correction was needed. We used the correction derived by Pich [44] in the slip flow regime, then the pressure drop was calculated as:

$$\Delta p = \frac{\Delta p_c}{1 + 0.998 * K_n * \left(\frac{p}{p - \Delta p_c}\right)\Big/(-0.75 - 0.5lna)} \tag{14}$$

with K_n: Knudson number $K_n = 2\lambda/d_f$, p: the ambient pressure, p_c: the pressure drop at continuum regime and we used equation (13) for Δp_c. After considering the slip correction the pressure drop decreased by 10 – 30% depending on the fiber diameter and solidity. For example, for the membrane with fiber diameter d_f of 0.2 μm and solidity α of 0.01 the pressure drop calculated by equation (14) is 70.2% of that calculated by equation (13).

4. Results and discussion

4.1. Aerodynamic property and equivalent diameters of plate-like GNPs

The airborne GNPs produced by atomizer were collected on the Nuclepore membranes and characterized by SEM. It could be seen that airborne GNPs still maintained the plate-like shape (Fig. 3a). The aerodynamic diameter distribution of GNPs was between 0.54 and 1.40 μm measured by APS and well fitted by the lognormal distribution (Fig. S1). As the APS minimum threshold of particle size determination was 0.54 μm (APS could detect particles smaller than 0.54 μm, but their sizes were not determined), thus the measured aerodynamic diameter started from 0.54 μm in the experiment. The thickness of GNPs was measured from SEM images (Fig. S2). The thickness distribution was fitted to a Gaussian distribution and the expectation of the thickness was about 66 nm (Fig. S3). According to the high-resolution SEM images, both of planar GNPs and folded GNPs could be observed (Fig. 3b-c). The folded structure was attributed to the large lateral size to thickness ratio and out-of-plane flexibility of GNPs. The folding behavior could be initiated by mechanical stimulation [45] or liquid evaporation [46], and stabilized by virtue of van der Waals forces. During the atomization process compressed air was used to break up GNPs suspension into aerosol. To investigate the effect of atomization on folding, the GNPs were collected on a silicon wafer close to the atomizer outlet and compared with the GNPs dispersed in the suspension. The airborne GNPs showed more folded configuration compared with the planar structure in the suspension (Fig. S4), indicating that the powerful mechanical stimulation during atomization could induce the folding behavior. Folded structure resulted in decreased geometric diameter and influenced particle penetration during filtration process.

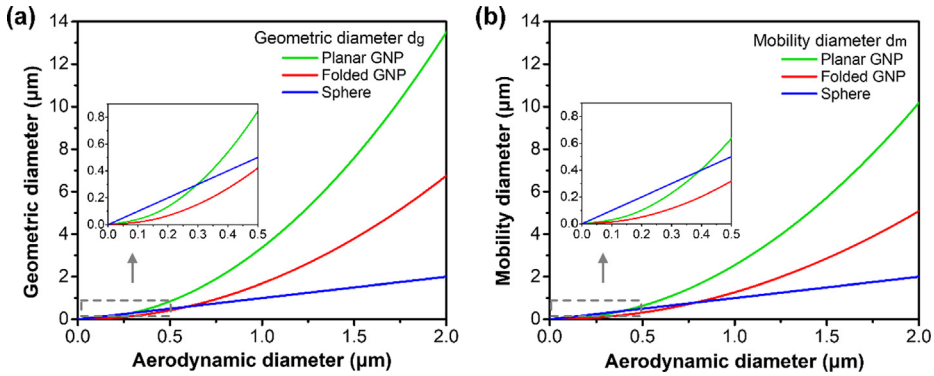

Fig. 4. Comparison of (a) geometric diameter d_g and (b) mobility diameter d_m between GNPs and spheres as a function of particle aerodynamic diameter d_a.

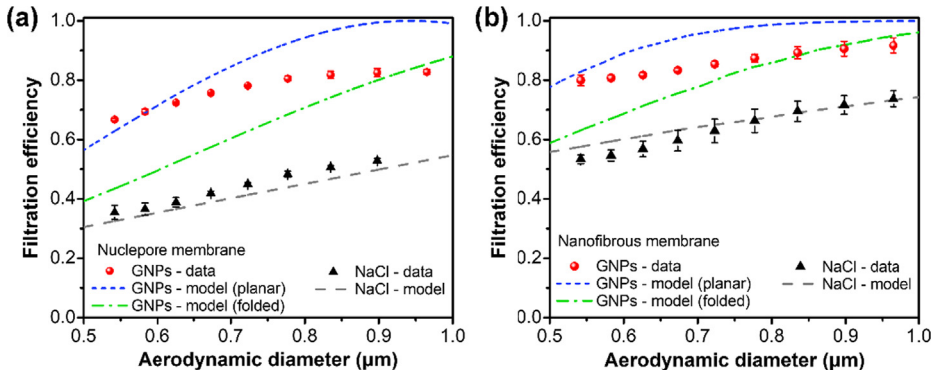

Fig. 5. Comparison of GNPs and NaCl particles capture efficiencies between experimental data and analytical model results at 5 cm s^{-1} with (a) Nuclepore membranes and (b) nanofibrous membranes.

The shape of a particle influenced its drag force and settling velocity, thus affecting the particle transportation and deposition. For plate-like GNPs, not only the geometrical diameter d_g, different equivalent diameters (aerodynamic diameter d_a and mobility diameter d_m) were also significant as they were adopted to describe diverse mechanisms in the filtration model. The equivalent diameters comparison between GNPs and spheres as a function of the aerodynamic diameter d_a is illustrated in Fig. 4. Three basic mechanisms were considered for aerosol filtration, including impaction, interception and diffusion. Impaction mechanism occurred as the particle was unable to adjust quickly enough to the curved stream lines and hit on the fiber due to the particle inertia. As impaction was affected by the particle aerodynamic behavior, the aerodynamic diameter d_a was used in the analytical model to calculate the efficiency due to impaction. Compared with the aerodynamic diameter d_a, the geometrical diameter d_g was a better approximation of the interception length due to the plate-like shape of GNPs. For small GNPs ($d_a < 0.29$ μm) the geometric diameter d_g was smaller than that of spheres, while for larger GNPs ($d_a > 0.29$ μm) d_g was much larger than spheres (Fig. 4a). The value of d_a was influenced by particle shape and density. The lateral size of small GNPs was not big enough to compensate the density effect, while for bigger GNPs the geometric diameter was much larger than spheres due to the large lateral size to thickness ratio. As the geometrical diameter d_g of GNPs was proportional to the square of aerodynamic diameter d_a (Equations (3) and (4)), d_g of GNPs increased with a faster rate than spheres. The geometric diameter disparity between GNPs and spheres became more obvious with the increment of particle size, suggesting that the platelet-shape effect was more pronounced for bigger particles. Diffusion mechanism contributed significantly to the collection of submicrometer-sized particles, and was governed by the mobility diameter d_m rather than the aerodynamic diameter d_a. According to the calculation results of Equations (6)–(8), d_m of GNPs ($d_a < 0.39$ μm) was smaller than spheres, while d_m of GNPs ($d_a > 0.39$ μm) was larger than spheres (Fig. 4b). In addition, the geometrical diameter d_g and mobility diameter d_m were also compared between planar GNPs and folded GNPs to evaluate the folding effect. We proposed an assumption that the totally folded GNP was a particle with half surface area and twofold thickness of the planar GNP. Therefore, the geometrical diameter d_g and mobility diameter d_m of folded GNPs were smaller than those of planar GNPs due to the reduced lateral size to thickness ratio. More analysis about the folding effect on the capture efficiency of GNPs is discussed in Section 4.2.

4.2. Filtration experiments and model results

The capture efficiencies of airborne plate-like GNPs and sphere-like NaCl particles were measured with Nuclepore membranes and nanofibrous membranes to evaluate the particle shape effect. Firstly, the capture efficiency was measured using Nuclepore filters with 3 μm pore size at 5 cm s^{-1}. The experimental data indicated the capture efficiency of GNPs was much higher than that of NaCl particles (Fig. 5a). With the particle aerodynamic diameter increasing from 0.54 to 0.96 μm, the capture efficiency of NaCl particles increased from 35.5% to 55.1%, and for GNPs the efficiency increased from 66.7% to 82.5%. The difference became more obvious with the increase of particle size, suggesting that the shape effect was more pronounced for bigger particles. For GNPs with aerodynamic diameter between 0.54 and 1.4 μm, the corresponding geometric diameters were between 1.0 and 6.7 μm. In this particle size range, filtration was dominated by interception and impaction mechanisms. The platelet-shaped GNPs had larger geometric diameter (about 2 – 4 times) than NaCl particles with the same aerodynamic diameter. Particles with larger lateral dimension were more prone to be intercepted during filtration process. Therefore, interception was the main mechanism that resulted in the efficiency difference between GNPs and NaCl particles. Instead of the aerodynamic diameter d_a, the geometric diameter d_g was a better approximation of the

interception length of GNPs and was used to calculate the interception efficiency in the capillary tube model. The analytical model results agreed well with the experimental data for NaCl particles, indicating that the capillary tube model was suitable for predicting the filtration efficiency of Nuclepore membranes. The experimental data were slightly lower than the model results for GNPs, the folded structure of GNPs observed from SEM might be the reason that led to this discrepancy. SEM images showed that not only planar GNPs, GNPs with folded structure also occurred owing to the large lateral size to thickness ratio and strong mechanical stimulation in atomization process. Due to the folding effect, the geometric diameter used in the model was larger than the actual interception length and resulted in an overestimation of the capture efficiency. To further consider the folding effect, the filtration efficiencies of planar GNPs and totally folded GNPs were analytically calculated. For GNPs with the aerodynamic diameter from 0.5 to 0.9 μm, the capture efficiency for folded GNPs decreased by 20 – 30% compared to planar GNPs due to the reduced particle geometric diameter. For small GNPs the experimental data were close to the model results of planar GNPs, while for bigger GNPs, the experimental data were closer to the model results of folded GNPs. As the particle lateral dimension influenced the torque generated by the drag force, larger GNPs were more deformable than smaller GNPs, thus the folding fraction raised with increasing GNPs size. This unique folding behavior resulted in higher penetration and should be given adequate attention for GNPs filtration.

Moreover, the capture efficiency of airborne GNPs and NaCl particles was measured using nanofibrous membranes. The nanofibrous membranes exhibited higher filtration efficiency than Nuclepore membranes for both GNPs and NaCl particles due to the nanoscale fiber diameter (Fig. 5b). The capture efficiency of GNPs was also higher than NaCl particles attributed to the larger interception length. For GNPs with the aerodynamic diameter of 0.54 μm, the capture efficiency was 80%, which was 50.1% higher than that of NaCl particles. The model results were consistent with the experimental data for NaCl particles implying that the single-fiber theory with slip effect consideration was suitable for predicting the filtration efficiency of nanofibrous membranes. The experimental efficiency was slightly lower than the model results for plate-like GNPs. Folding resulted in smaller geometrical diameter and lower capture efficiency than the planar GNPs. The experimental efficiency of GNPs was between the model results of planar GNPs and totally folded GNPs, indicating that not only planar GNPs, but also folded GNPs existed. Similar to Nuclepore membranes, the capture efficiency of GNPs with nanofibrous membranes was also higher than NaCl particles, further confirming that particle shape was a significant factor influencing particle transportation during filtration.

4.3. Particle shape effect on GNPs theoretical penetration

In order to systematically evaluate the penetration difference between GNPs and spheres, the penetration of particles with aerodynamic diameter from 0.07 to 10 μm was analytical calculated. The effects of the membrane structural parameters (Nuclepore membrane pore radius r_0, nanofiber diameter d_f, solidity α) on the penetration were also evaluated. Firstly, the effect of pore radius r_0 of Nuclepore membrane was evaluated with r_0 = 1.5, 2.5 and 4 μm. The other parameters were the same as the Nuclepore membrane used in the experiment with the porosity P = 0.14 and the thickness t = 9.9 μm, and face velocity U_0 = 5 cm s^{-1}. The calculated penetration curves for GNPs and spheres are shown in Fig. 6a. The penetration of GNPs was lower than spheres with the particle aerodynamic diameter from 0.07 to 10 μm. Different mechanisms had diverse dependencies on particle size. For very small particles, the dominant diffusion deposition was similar for GNPs and spheres and the particle shape effect was not obvious. For particles with the aerodynamic diameter > 2 μm, the penetration approached to zero for both GNPs and spheres. In the intermediate size range, interception mechanism played a significant role and the penetration disparity between GNPs and spheres was notable. The penetration difference ΔPenetration was calculated based on the equation derived by Wang [47], and the corresponding particle aerodynamic diameter d_a was referred to as the most differentiating particle size (MDPS):

$$\Delta Penetration(d_a) = Penetration(sphere, d_a) - Penetration(GNP, d_a) \quad (15)$$

The maximum ΔPenetration and MDPS depended on the membrane parameters such as fiber diameter, solidity, thickness; particle parameters such as particle shape and density; filtration parameters such as face velocity. The maximum ΔPenetration between planar GNPs and spheres and corresponding MDPS are shown in Table S1. The maximum ΔPenetration increased with pore radius and reached 46.4% at r_0 = 4 μm. The corresponding MDPS also rose from 0.844 μm (r_0 = 1.5 μm) to 1.378 μm (r_0 = 4 μm). These results suggested that small pore radius should be used to differentiate small GNPs and spheres, and large pore radius should be used to differentiate big GNPs and spheres. There also existed a particle size range where the particle penetration was maximum, and the corresponding particle size was termed as the most penetrating particle size (MPPS). The MPPS was smaller than the MDPS on the penetration curves. The penetrations of GNPs and spheres with aerodynamic diameter of 0.244 μm were approximately the same. For particles smaller than 0.244 μm, GNPs had more diffusion and less interception depositions than spheres due to the smaller mobility diameter and geometric diameter. As diffusion was the dominant deposition mechanism for small particles, the total penetration of GNPs was lower. With the increase of aerodynamic diameter, the geometric diameter of GNPs increased much faster than spheres, resulting in higher interception efficiency, thus the total penetration of GNPs was still lower than spheres. To investigate the folding effect on GNPs transportation, the penetration curves of planar and folded GNPs were compared and the influence of r_0 was analyzed. The calculated penetration curves with particle aerodynamic diameter from 0.07 to 10 μm are shown in Fig. 6b. Folded GNPs had lower penetration than planar GNPs with the particle aerodynamic diameter smaller than 0.3 μm and higher penetration for particles > 0.3 μm. Folding led to smaller mobility diameter, resulting in enhanced diffusion deposition. As diffusion mechanism was more important for smaller particles, the penetration of folded GNPs with d_a < 0.3 μm was lower. Folded GNPs also had smaller geometrical diameter resulting in decreased interception efficiency. As interception was the dominant mechanism for bigger particles, the penetration of folded GNPs with d_a > 0.3 μm was higher. The maximum ΔPenetration between planar GNPs and folded GNPs and corresponding MDPS are shown in Table S2. With the increase of r_0 from 1.5 to 4 μm, the maximum ΔPenetration was kept at about 25%, while the corresponding MDPS increased from 0.731 to 1.180 μm. The maximum ΔPenetration between planar and folded GNPs was smaller than that between planar GNPs and spheres, indicating that compared with shape deformation caused by folding, the shape difference between plate-like and spherical particles was more significant and affected maximum ΔPenetration during filtration.

As the fibrous membrane has a different structure from the Nuclepore membrane, the effects of fiber diameter d_f and solidity α on the capture efficiency of GNPs and spheres were also evaluated. Firstly, the effect of d_f on particle penetration was investigated by analytical calculation with d_f = 0.20, 0.45 and 1 μm. The other membrane parameters were the same as the PAN electrospun membrane with the solidity α = 0.03, thickness t = 6 μm, and face velocity U_0 = 5 cm s^{-1}. The calculated penetration curves are shown in Fig. 7a-b. The maximum ΔPenetration between planar GNPs and spheres enhanced significantly with increasing d_f and reached 53.2% at d_f = 1 μm. The corresponding MDPS also increased obviously from 0.385 μm (d_f = 0.2 μm) to 1.491 μm (d_f = 1 μm). The increased MDPS was due to the fact that the interception deposition was significant when the particle size was comparable to the fiber diameter. If the interception parameter R was too small, the effect of interception could hardly be

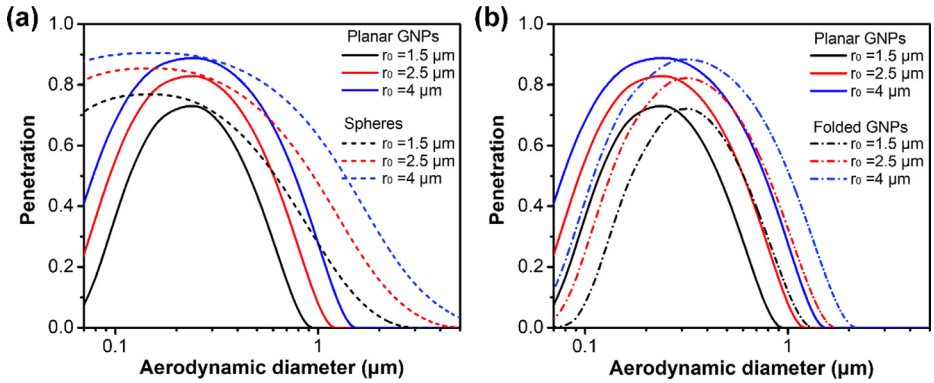

Fig. 6. Penetration values from model calculation for Nuclepore membrane with pore radius r_0 of 1.5, 2.5 and 4 μm between (a) planar GNPs and spheres, (b) planar GNPs and folded GNPs.

observed. The MPPS of fibrous membrane increased with increasing d_f, which was consistent with the results in the literature. The MPPS could also be calculated based on Equation (16) [48]. The calculated MPPSs of fibrous membranes with d_f of 0.20, 0.45 and 1 μm were 0.098, 0.139 and 0.199 μm, respectively.

$$\hat{d} = 0.885\left[\left(\frac{Ku}{1-\alpha}\right)\left(\frac{\sqrt{\lambda}kT}{\mu}\right)\left(\frac{d_f^2}{U_0}\right)\right]^{2/9} \tag{16}$$

Additionally, the influence of d_f on the penetration of planar and folded GNPs were evaluated. The maximum penetration of folded GNPs was slightly lower than planar GNPs and the corresponding MPPS was larger. The maximum ΔPenetration between planar and folded GNPs increased with the fiber diameter and reached 27.5% at $d_f = 1$ μm. The corresponding MDPS increased from 0.344 μm (d_f = 0.2 μm) to 1.142 μm (d_f = 1 μm), and the MDPS was larger than the MPPS. The reason was that the maximum ΔPenetration was achieved as the penetration of folded GNPs began to reduce from the maximum penetration, and at the same time the penetration of planar GNPs approached zero due to the high interception deposition. The maximum ΔPenetration between planar GNPs and spheres was larger than that between planar and folded GNPs.

Furthermore, the effect of fibrous membrane solidity α on GNPs penetration was investigated with α = 0.03, 0.05 and 0.1 (Fig. 7c-d). The other parameters were the same as the PAN electrospun membrane with fiber diameter d_f = 0.45 μm, thickness t = 6 μm, and face velocity U_0 = 5 cm s^{-1}. The calculated MPPSs (Equation (15)) of fibrous membranes with α of 0.03, 0.05 and 0.1 μm were 0.139, 0.140 and

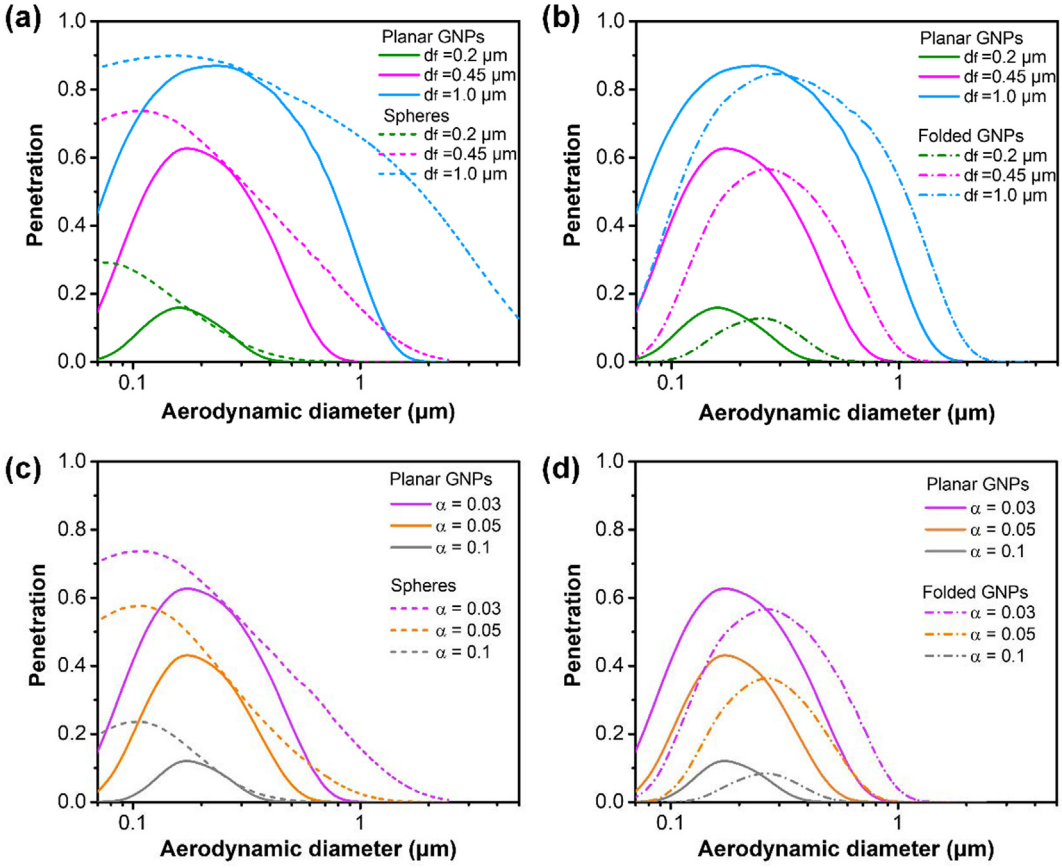

Fig. 7. Penetration values from model calculation for fibrous membrane with fiber diameter d_f of 0.2, 0.45 and 1.0 μm and solidity α of 0.03, 0.05 and 0.1 between (a) (c) planar GNPs and spheres, (b) (d) planar GNPs and folded GNPs.

0.142 μm, respectively, indicating that the solidity had minor effect on the MPPS. The maximum ΔPenetration between planar GNPs and spheres was 23.5% at $\alpha = 0.03$ and decreased to 10.6% at $\alpha = 0.05$. The corresponding MDPS decreased from 0.689 to 0.545 μm. The maximum ΔPenetration between planar GNPs and folded GNPs was 20.7% ($\alpha = 0.03$) and decreases to 14.4% ($\alpha = 0.05$). The corresponding MDPS also decreased from 0.571 to 0.456 μm. The comparison between the maximum ΔPenetration by adjusting fiber diameter or solidity indicated that fiber diameter was a more significant parameter influencing the ΔPenetration between GNPs and spheres.

4.4. Analysis for the Q_f of Nuclepore and nanofibrous membranes

The adjustment of the membrane structural parameters causes the change of both penetration P and pressure drop Δp. A useful criterion for evaluating the filtration performance of various types of filters with different parameters is the quality factor Q_f, (also known as the figure of merit) which is described as:

$$Q_f = -\ln(P)/\Delta p \tag{17}$$

The Q_f depicts the ratio between filtration efficiency and pressure drop, and larger Q_f indicates better filtration property. It should be noted that the comparison of Q_f must be made at the same particle size and face velocity. The relevant significance of efficiency and pressure drop may be valued differently in different applications, thus there are various ways to assess the comprehensive filtration performance of the filter, and we focus on the Q_f in this study.

Firstly, the effect of pore radius r_0 on the Q_f of GNPs with Nuclepore membrane was evaluated (Fig. 8a). As the geometric diameter d_g of GNPs ($d_a = 1.63$ μm) was 9 μm, the capture efficiency would be 100% when the pore radius r_0 was smaller than 4.5 μm, therefore, the Q_f of GNPs ($d_a = 1.63$ μm) in Fig. 8a started from $r_0 = 5$ μm. Increasing r_0 resulted in lower efficiency and lower pressure drop. As the pressure drop decreased at a faster rate and outweighed the decrease of efficiency, the Q_f enhanced with increasing r_0. The Q_f of GNPs ($d_a = 0.24$ μm) increased obviously from 0.011 Pa^{-1} ($r_0 = 3$ μm) to 0.086 Pa^{-1} ($r_0 = 6$ μm), which raised by about 6.8 times. The Q_f for GNPs ($d_a = 1.22$ μm) enhanced by about 5.1 times with r_0 increasing from 3 to 6 μm, at the same time the filtration efficiency only descended by 27%. Appropriately increasing r_0 could improve the Q_f while still maintain the relatively high filtration efficiency. In addition, the Q_f values of GNPs and spherical particles were also compared to evaluate the particle shape effect. The Q_f of GNPs was higher than spheres with the same aerodynamic diameter, and the disparity was more obvious for bigger particles. The Q_f of GNPs with $d_a = 0.54$ μm was 1.6 times that of spheres, and the Q_f of GNPs with $d_a = 1.22$ μm was 4.9 times that of spheres at $r_0 = 3$ μm. On one hand, as the pressure drop was only influenced by filtration parameters and membrane structural parameters, the pressure drop was the same for GNPs and spheres. On the other hand, the filtration efficiency of GNPs was higher than spheres due to the larger interception length, thus the Q_f of GNPs was higher than spherical particles. In summary, with the increase of membrane pore radius, the Q_f of both GNPs and spheres showed ascendant tendency, but the Q_f value of GNPs was much larger than spheres.

Secondly, the influence of nanofiber diameter d_f on the Q_f is illustrated in Fig. 8b. For smaller GNPs ($d_a = 0.24$ μm), the Q_f decreased as d_f decreases. For larger GNPs ($d_a = 0.54$, 1.22 and 1.63 μm), the Q_f increased with the decrease of d_f. The calculation results of Equation (13) showed that the pressure drop increased obviously when d_f decreased from micrometers to nanometers. With the decrease of d_f the single-fiber efficiency owing to diffusion increased at a lower rate than the pressure drop, resulting in the slightly descendent Q_f for small GNPs. For larger GNPs the combined filtration efficiency due to interception and inertial impaction raised faster than the pressure drop, leading to the ascendant Q_f. The Q_f of GNPs showed the similar trend as spheres. Similar results regarding the effect of d_f on the Q_f of fibrous membranes with spherical particles were reported [49]. Hinds [34] also indicated that with the decrease of d_f the Q_f declined for spherical particles with $d_g < 100$ nm, but enhanced for particles with $d_g > 200$ nm. Smaller fiber diameter brought out higher Q_f for bigger GNPs, nevertheless, during practical filtration applications, the aim was usually to capture particles of a specific size, especially the MPPS. As the MPPS of GNPs with nanofibrous membrane was about 0.2 – 0.3 μm, decreasing fiber diameter did not improve the Q_f for GNPs in this size range. The Q_f of fibrous membrane was not only influenced by fiber diameter, but also affected by fiber morphology. Optimizing fiber morphology also contributed to the improvement of Q_f [50,51].

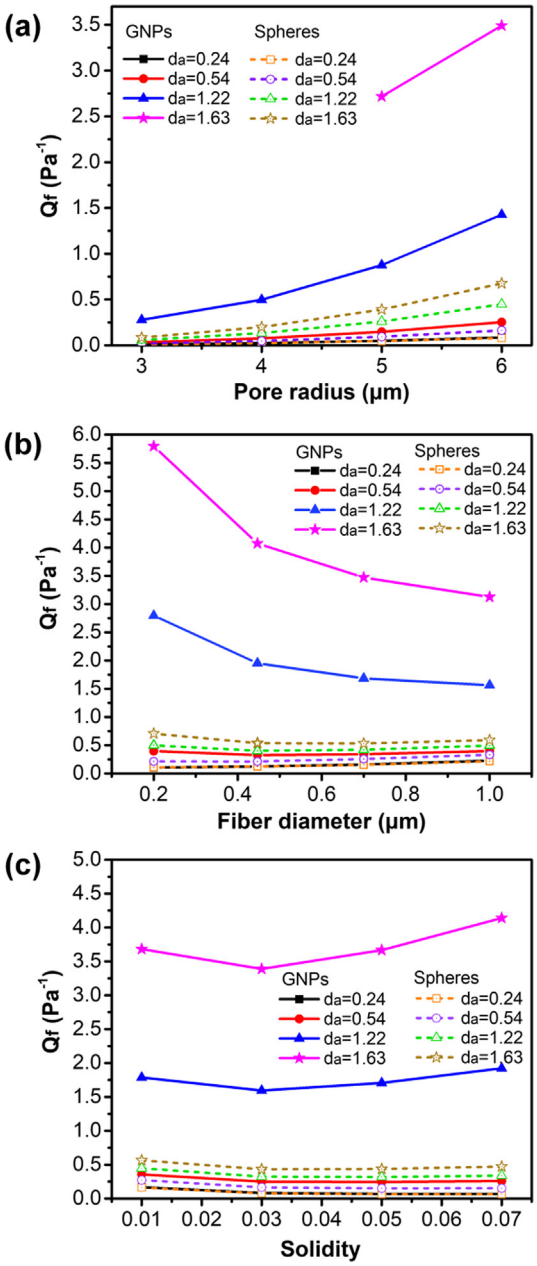

Fig. 8. The quality factor Q_f of GNPs and spheres with different aerodynamic diameters d_a with (a) Nuclepore membrane pore radius r_0 of 3, 4, 5 and 6 μm, (b) fiber diameter d_f of 0.2, 0.45, 0.7 and 1 μm (solidity $\alpha = 0.01$), (c) fibrous membrane solidity α of 0.01, 0.03, 0.05 and 0.07 (fiber diameter $d_f = 0.7$ μm).

In addition, the influence of nanofiber membrane solidity α on the Q_f was also investigated (Fig. 8c). The Q_f for smaller GNPs ($d_a = 0.24$) was observed to decrease as the solidity increased, whereas the Q_f for bigger GNPs ($d_a = 1.22$ and 1.63 μm) first decreased at small solidity

and then enhanced with increasing solidity. The reason was that at small solidity with the increase of solidity the pressure drop increased faster than filtration efficiency, resulting in the descend Q_f. Then with the further increase of solidity, the combined efficiency due to interception and inertial impaction for bigger particles overwhelmed the increment of pressure drop and led to the improved Q_f. The Q_f of GNPs showed the similar trend as spheres, but the Q_f of GNPs was much larger than spheres especially for bigger particles. The reason might be that the plate-like GNPs had larger geometrical diameter than spheres. With the increase of particle size, the interception efficiency of GNPs increased faster attributed to the larger geometrical diameter and outweighed the pressure drop augmentation.

5. Conclusions

In summary, the aerodynamics and filtration mechanisms of airborne GNPs with plate-like shape and folded structure were studied. The equivalent diameters of GNPs were derived from the basic aerodynamic principles of oblate spheroids. For GNPs and spheres with the same aerodynamic diameter d_a ($d_a > 0.39$ μm), the geometric diameter d_g and mobility diameter d_m of GNPs was much larger than spheres due to the large lateral size to thickness ratio. Plate-like GNPs showed higher capture efficiency than sphere-like NaCl particles due to the larger interception length. Compared to planar GNPs, the capture efficiency for folded GNPs with aerodynamic diameter of 0.5 – 0.9 μm decreased 20 – 30% due to the reduced geometric diameter. In addition, the effects of membrane structural parameters (Nuclepore membrane pore radius, fiber diameter and solidity) on the particle penetration were systematically evaluated by analytical calculation. The comparison of the maximum ΔPenetration by adjusting nanofiber diameter and solidity indicated that nanofiber diameter was a more significant parameter influencing the penetration disparity between GNPs and spheres. Furthermore, the effect of membrane structural parameters on the Q_f was also investigated for better membrane design with optimized filtration performance. With the given parameters in our experiments, the analytical model calculation demonstrated that the Q_f value of GNPs was larger than spheres. This study not only reveals the unique aerodynamic property of plate-like GNPs and the effect on particle transportation and deposition, but also provides a useful guide for better Nuclepore and nanofibrous membranes structure design to optimize filtration performance of plate-like particles.

CRediT authorship contribution statement

Hanchao Gao: Conceptualization, Methodology, Investigation, Writing - original draft. **Weidong He:** Validation, Formal analysis. **Ranxue Yu:** Data curation, Investigation. **Tobias Hammer:** Data curation, Investigation. **Guangbiao Xu:** Supervision, Writing - review & editing. **Jing Wang:** Supervision, Writing - review & editing, Funding acquisition.

Declaration of Competing Interest

The authors declare that they have no known competing financial interests or personal relationships that could have appeared to influence the work reported in this paper.

Acknowledgements

This work is partially supported by Swiss National Science Foundation (grant number 310030_169207) and Center for Filtration Research at University of Minnesota. The authors also thank the financial aid from China Scholarship Council.

Appendix A. Supplementary material

Supplementary data to this article can be found online at https://doi.org/10.1016/j.seppur.2020.117293.

References

[1] Q. He, S. Wu, Z. Yin, H. Zhang, Graphene-based electronic sensors, Chem. Sci. 3 (2012) 1764.
[2] H. Kim, J.-H. Ahn, Graphene for flexible and wearable device applications, Carbon 120 (2017) 244–257.
[3] A. Idowu, B. Boesl, A. Agarwal, 3D graphene foam-reinforced polymer composites – A review, Carbon 135 (2018) 52–71.
[4] R. Imani, F. Mohabatpour, F. Mostafavi, Graphene-based nano-carrier modifications for gene delivery applications, Carbon 140 (2018) 569–591.
[5] M. Pelin, S. Sosa, M. Prato, A. Tubaro, Occupational exposure to graphene based nanomaterials: risk assessment, Nanoscale 10 (2018) 15894–15903.
[6] B. Fadeel, C. Bussy, S. Merino, E. Vazquez, E. Flahaut, F. Mouchet, L. Evariste, L. Gauthier, A.J. Koivisto, U. Vogel, C. Martin, L.G. Delogu, T. Buerki-Thurnherr, P. Wick, D. Beloin-Saint-Pierre, R. Hischier, M. Pelin, F. Candotto Carniel, M. Tretiach, F. Cesca, F. Benfenati, D. Scaini, L. Ballerini, K. Kostarelos, M. Prato, A. Bianco, Safety assessment of graphene-based materials: focus on human health and the environment, ACS Nano 12 (2018) 10582–10620.
[7] L. Schlagenhauf, B.T. Chu, J. Buha, F. Nuesch, J. Wang, Release of carbon nanotubes from an epoxy-based nanocomposite during an abrasion process, Environ. Sci. Technol. 46 (2012) 7366–7372.
[8] J. Wang, L. Schlagenhauf, A. Setyan, Transformation of the released asbestos, carbon fibers and carbon nanotubes from composite materials and the changes of their potential health impacts, J. Nanobiotechnol. 15 (2017) 15.
[9] K. Starost, E. Frijns, J. Van Laer, N. Faisal, A. Egizabal, C. Elizextea, M. Blazquez, I. Nelissen, J. Njuguna, Assessment of nanoparticles release into the environment during drilling of carbon nanotubes/epoxy and carbon nanofibres/epoxy nanocomposites, J. Hazard. Mater. 340 (2017) 57–66.
[10] L. Schlagenhauf, B. Kianfar, T. Buerki-Thurnherr, Y.Y. Kuo, A. Wichser, F. Nuesch, P. Wick, J. Wang, Weathering of a carbon nanotube/epoxy nanocomposite under UV light and in water bath: impact on abraded particles, Nanoscale 7 (2015) 18524–18536.
[11] L. Schlagenhauf, Y.-Y. Kuo, Y.K. Bahk, F. Nüesch, J. Wang, Decomposition and particle release of a carbon nanotube/epoxy nanocomposite at elevated temperatures, J. Nanopart. Res. 17 (2015) 440.
[12] X. Ren, J. Li, C. Chen, Y. Gao, D. Chen, M. Su, A. Alsaedi, T. Hayat, Graphene analogues in aquatic environments and porous media: dispersion, aggregation, deposition and transformation, Environ. Sci-Nano 5 (2018) 1298–1340.
[13] K. He, G. Chen, G. Zeng, M. Peng, Z. Huang, J. Shi, T. Huang, Stability, transport and ecosystem effects of graphene in water and soil environments, Nanoscale 9 (2017) 5370–5388.
[14] W.C. Su, B.K. Ku, P. Kulkarni, Y.S. Cheng, Deposition of graphene nanomaterial aerosols in human upper airways, J. Occup. Environ. Hyg. 13 (2016) 48–59.
[15] J. Wang, D. Thompson, D.Y.H. Pui, Integrative filtration research and sustainable nanotechnology, Particuology 11 (2013) 5–13.
[16] W.D. He, Y.B. Zhao, F.Z. Jiang, Y.H. Gu, H.C. Gao, J.X. Liu, J. Wang, Filtration performance and charge degradation during particle loading and reusability of charged PTFE needle felt filters, Sep. Purif. Technol. 233 (2020).
[17] Z.Y. Pan, Y. Liang, M. Tang, Z.X. Sun, J. Hu, J. Wang, Simulation of performance of fibrous filter media composed of cellulose and synthetic fibers, Cellulose 26 (2019) 7051–7065.
[18] H.C. Gao, W.D. He, Y.B. Zhao, D.M. Opris, G.B. Xu, J. Wang, Electret mechanisms and kinetics of electrospun nanofiber membranes and lifetime in filtration applications in comparison with corona-charged membranes, J. Membrane Sci. 600 (2020).
[19] C.Y. Tien, J.P. Chen, S. Li, Z.Y. Li, Y.M. Zheng, A.S. Peng, F. Zhou, C.J. Tsai, S.C. Chen, Experimental and theoretical analysis of loading characteristics of different electret media with various properties toward the design of ideal depth filtration for nanoparticles and fine particles, Sep. Purif. Technol. 233 (2020).
[20] M. Tang, S.C. Chen, D.Q. Chang, X.F. Xie, J. Sun, D.Y.H. Pui, Filtration efficiency and loading characteristics of PM2.5 through composite filter media consisting of commercial HVAC electret media and nanofiber layer, Sep. Purif. Technol. 198 (2018) 137–145.
[21] M. Wang, B. Gao, D. Tang, Review of key factors controlling engineered nanoparticle transport in porous media, J. Hazard. Mater. 318 (2016) 233–246.
[22] A. Feigley, mathematical model for deposition of asbestos in a fibrous filter, Clean Air 9 (1975) 67–71.
[23] S.C. Chen, J. Wang, Y.K. Bahk, H. Fissan, D.Y.H. Pui, Carbon nanotube penetration through fiberglass and electret respirator filter and nuclepore filter media: experiments and models, Aerosol Sci. Technol. 48 (2014) 997–1008.
[24] Y.K. Bahk, J. Wang, Filtration and length determination of airborne carbon nanotubes in the submicrometer range using nanofiber filters, Aerosol Air Qual. Res. 14 (2014) 1352–1359.
[25] Y.K. Bahk, J. Buha, J. Wang, Determination of geometrical length of airborne carbon nanotubes by electron microscopy, model calculation, and filtration method, Aerosol Sci. Technol. 47 (2013) 776–784.
[26] J. Wang, S.C. Kim, D.Y.H. Pui, Carbon nanotube penetration through a screen filter: numerical modeling and comparison with experiments, Aerosol Sci. Technol. 45 (2011) 443–452.

[27] X. Meng, M. Li, Z. Kang, X. Zhang, J. Xiao, Mechanics of self-folding of single-layer graphene, J. Phys. D Appl. Phys. 46 (2013) 055308.
[28] H. Li, M. Li, Z. Kang, Mechanics of the scrolling and folding of graphene, Nanotechnology 29 (2018) 245604.
[29] S.T. Yang, Y. Chang, H. Wang, G. Liu, S. Chen, Y. Wang, Y. Liu, A. Cao, Folding/aggregation of graphene oxide and its application in Cu2+ removal, J. Colloid Interf. Sci. 351 (2010) 122–127.
[30] A. Patanaik, V. Jacobs, R.D. Anandjiwala, Performance evaluation of electrospun nanofibrous membrane, J. Membrane Sci. 352 (2010) 136–142.
[31] C.-H. Hung, W.-W.-F. Leung, Filtration of nano-aerosol using nanofiber filter under low Peclet number and transitional flow regime, Sep. Purif. Technol. 79 (2011) 34–42.
[32] H. Gao, Y. Yang, O. Akampumuza, J. Hou, H. Zhang, X. Qin, A low filtration resistance three-dimensional composite membrane fabricated via free surface electrospinning for effective PM2.5 capture, Environ. Sci-Nano 4 (2017) 864–875.
[33] Y.-Y. Kuo, F.C. Bruno, J. Wang, Filtration performance against nanoparticles by electrospun nylon-6 media containing ultrathin nanofibers, Aerosol Sci. Technol. 48 (2014) 1332–1344.
[34] W.C. Hinds, Aerosol Technology: properties, behavior and measurement of airborne particles, Wiley-interscience, United States of America, 1999.
[35] Y.-S. Cheng, H.-C. Yeh, M.D. Allen, Physical characterization and aerodynamic behavior of plate-like particles Ann. occup, Hyg. 32 (1988) 369–378.
[36] Y.-S. Cheng, H.-C. Yeh, M.D. Allen, Dynamic shape factor of a plate-like particle, Aerosol Sci. Technol. 8 (1988) 109–123.
[37] T.F. Tomb, M. Corn, Comparison of equivalent spherical volume and aerodynamic diameters for irregularly shaped particles, Am. Ind. Hyg. Assoc. J. 34 (2010) 13–24.
[38] A. Schinwald, F.A. Murphy, A. Jones, W. MacNee, K. Donaldson, Graphene-based nanoplatelets: a new risk to the respiratory system as a consequence of their unusual aerodynamic properties, ACS Nano 6 (2012) 736–746.
[39] R.Y.S. Lai, L.F. Mockros, The stokes-flow drag on prolate and oblate spheroids during axial translatory accelerations, J. Fluid Mech. 52 (2006) 1–15.
[40] N.A. Fuchs, The mechanics of aerosols, Institue of Scientific Information, Moscow, 1955.
[41] K.R. Spurny, J.P. Lodge, E.R. Frank, D.C. Sheesley, Aerosol filtration by means of nuclepore filters structural and filtration properties, Environ. Sci. Technol. 3 (1969) 453–464.
[42] L. Bao, K. Seki, H. Niinuma, Y. Otani, R. Balgis, T. Ogi, L. Gradon, K. Okuyama, Verification of slip flow in nanofiber filter media through pressure drop measurement at low-pressure conditions, Sep. Purif. Technol. 159 (2016) 100–107.
[43] C.N. Davies, Air filtration, Academic Press, London, 1973.
[44] J. Pich, Pressure characteristics of fibrous aerosol filters, J. Colloid Interf. Sci. 37 (1971) 912–917.
[45] J. Zhang, J. Xiao, X. Meng, C. Monroe, Y. Huang, J.M. Zuo, Free folding of suspended graphene sheets by random mechanical stimulation, Phys. Rev. Lett. 104 (2010) 166805.
[46] Q. Liu, B. Xu, Two- and three-dimensional self-folding of free-standing graphene by liquid evaporation, Soft Matter 14 (2018) 5968–5976.
[47] J. Wang, Effects of particle size and morphology on filtration of airborne nanoparticles, Kona Powder Part. J. (2013) 256–266.
[48] K.W. Lee, B.Y.H. Liu, On the minimum efficiency and the most penetrating particle size for fibrous filters, J. Air Pollut. Control Assoc. 30 (1980) 377–381.
[49] J. Wang, S.C. Kim, D.Y.H. Pui, Figure of merit of composite filters with micrometer and nanometer fibers, Aerosol Sci. Technol. 42 (2008) 722–728.
[50] J. Su, G. Yang, C. Cheng, C. Huang, H. Xu, Q. Ke, Hierarchically structured TiO2/PAN nanofibrous membranes for high-efficiency air filtration and toluene degradation, J. Colloid Interf. Sci. 507 (2017) 386–396.
[51] P. Li, Y. Zong, Y. Zhang, M. Yang, R. Zhang, S. Li, F. Wei, In situ fabrication of depth-type hierarchical CNT/quartz fiber filters for high efficiency filtration of submicron aerosols and high water repellency, Nanoscale 5 (2013) 3367–3372.